Preprints of the 21st IFAC World Congress (Virtual)
Berlin, Germany, July 12-17, 2020

A model to control self-erecting tower cranes with elastic structure

Matthias Thomas * **Oliver Sawodny** *

* *Institute for System Dynamics, University of Stuttgart, Germany*
(e-mail: thomas@isys.uni-stuttgart.de, sawodny@isys.uni-stuttgart.de).

Abstract: Control of large-scale tower cranes is still an open research field. Due to their lightweight structure and their large geometry structural deformations occur and need to be considered for anti-sway feedback control. Especially, for self-erecting tower cranes no proper model has been published yet. In this paper, a flexible multi-body model for this type of crane is derived and a modal analysis is performed. The results are compared to measurement data of an industrial tower crane.

Keywords: discretization, model reduction, modal analysis, validation, industrial crane

1. INTRODUCTION

Cranes are used to transport heavy goods hanging on a rope. They are usually categorized according to their degrees of freedom. The main categories are rotary and overhead cranes. The latter have a trolley moving over a horizontal girder, which is either mounted on a bridge (bridge crane) or fixed on a mobile crane structure which moves on floor level (gantry crane). Rotary cranes are distinguished in tower cranes having a vertical tower and horizontal jib and boom cranes having a sloped boom which can be luffed. The payload can be hoisted by a rope which is either suspended at the boom tip or on a trolley moving along the horizontal jib of a tower crane.

Crane control aims at the reduction of payload pendulum oscillations during operation to increase productivity and safety. An overview of modeling and control of cranes, which are in general underactuated machines, is given by Abdel-Rahman et al. (2003) and Ramli et al. (2017). Most publications address overhead cranes whose dynamical behavior is typically modeled as a single or double pendulum with planar motion of the rope suspension point. In comparison, control of rotary cranes is more difficult because the rotation of a jib or boom respectively yields nonlinear kinematics. Nevertheless, many different control approaches of boom and tower cranes are analyzed using rigid crane models, e.g. open-loop feedforward control by Vaughan et al. (2010), gain-scheduled state feedback control by Omar and Nayfeh (2003), flatness-based control by Neupert et al. (2006), or model-predicitve control by Arnold et al. (2005) and Graichen et al. (2010), or combinations by Neupert et al. (2010).

Ju et al. (2006) analyzed the dynamical behavior of top-slewing tower cranes applying the finite element method and concluded that besides payload pendulum oscillations the first few mode shapes of the crane structure are relevant to describe the dynamical behavior. However, only few publications deal with control of flexible tower cranes. Takagi and Nisimura (1999), Jerman et al. (2004), Devesse (2012), Schlott et al. (2016) modeled tower cranes using rigid bodies with flexible links and Yang et al. (2007), Tinkir et al. (2011), and Rauscher and Sawodny (2017) used Euler-Bernoulli-beams to consider elastic jib deformations. The publication by Yang et al. (2007) led to discussions about controversial assumptions commented by Zrnić and Bošnjak (2008). Most investigations on control of rotary cranes are made on scaled laboratory test rigs and publications about industrial cranes are very rare as pointed out by Ramli et al. (2017). To the best of the authors' knowledge, only the publication by Rauscher and Sawodny (2020) shows control design and measurement results for an industrial tower crane.

Tower cranes are distinguished in top-slewing and bottom-slewing cranes depending on the slewing drive's position. The latter are typically called self-erecting cranes. Both types of tower cranes have different geometry and dynamical behavior. Since existing tower crane models do not describe the geometry of self-erecting tower cranes, either because they are derived to control laboratory tower cranes with simpler geometry or because they describe top-slewing tower cranes, according to the author's knowledge, no proper dynamical model for control of self-erecting industrial tower cranes with elastic structure was published until today. The authors assume that the consideration of elastic deformations is essential for anti-sway control of all types of industrial tower cranes. Therefore, a proper dynamical model for self-erecting tower cranes is derived in this paper and validated using experimental data of an industrial crane.

The equations of motion are derived in Section 2 and the required model parameters are discussed in Section 3 including an parameter optimization. The dynamical behavior of the elastic crane structure is analyzed in Section 4 and the results are compared to measurement data of an industrial tower crane. Finally, a conclusion is given in Section 5.

2. MODELING

We focus on bottom-slewing tower cranes with elastic structure. Bottom-slewing means that the slewing drive's position is at the bottom of the tower. Typically, the entire crane is located on a platform which is driven by an asynchronous motor and thus the geometry differs significantly from top-slewing tower cranes, which have

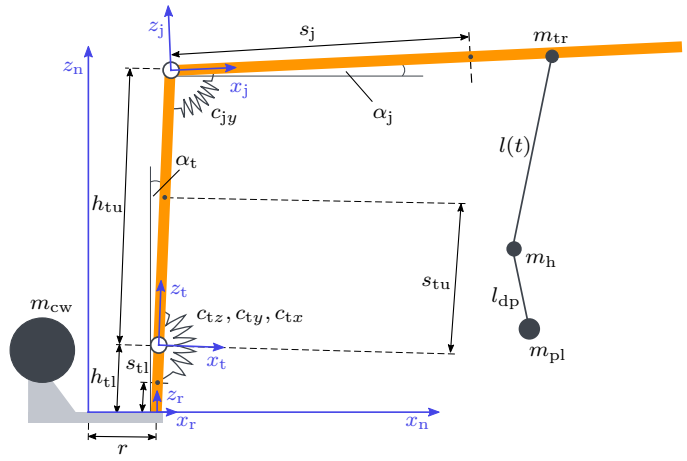

Fig. 1. Model of the self-erecting tower crane.

a rotating jib and a fixed tower. Additionally, the tower and jib of a bottom-slewing tower crane are often slightly sloped and the tower's longitudinal axis is not identical to the rotational axis as it is the case for a top-slewing crane with a vertical tower. Whereas the counter weight is positioned at the crane platform for bottom-slewing tower cranes, top-slewing cranes usually have a counter-jib. It is clear, that the differences in geometry will lead to different dynamical behavior.

The resulting model of the bottom-slewing tower crane is shown in Fig. 1. The tower is represented by two rigid bodies with heights h_{tu} and h_{tl}. The centers of mass are at positions s_{tu} and s_{tl}. Whereas the lower part of the tower is fixed at the crane platform, a (virtual) spherical joint allows rotations of the upper part around all three axes representing structural deformations. The elasticity is considered by discrete springs with stiffnesses c. The guying, which is not modeled in detail and not shown in Fig. 1, allows a rigid body motion of the jib in radial direction. The elasticity of jib and guying is modeled by a discrete spring. The jib's center of mass is s_{j}. Whereas the jib is rigid in radial direction, jib's deformation in slewing direction is modeled as bending of an Euler-Bernoulli-beam. In general, tower cranes are more elastic in slewing direction and therefore it is essential to model deformations in this direction in more detail. Counterweight, trolley, hook and payload are represented by point masses m_{cw}, m_{tr}, m_{h}, and m_{pl} whereas the ropes and the platform masses are neglected. The distance of the tower's bottom point to the rotation axis z_{n} is r. It is tilted by the angle α_{t}. Jib's tilt angle is α_{j} and its center of mass is at s_{tl}. The rope length $l(t)$ is actuated whereas the lower rope with length l_{dp} is constant for each payload.

2.1 Kinematics

The mechanical degrees of freedom describing the dynamical behavior of the elastic crane structure and pendulum motions are

$$\begin{aligned}\mathbf{q}_{\mathrm{m}} =&[\nu_z(t), \nu_y(t), \nu_x(t), \beta(t), v(x_{\mathrm{j}}, t), \varphi_x(t), \varphi_y(t),\\ &\phi_x(t), \phi_y(t)]^{\mathrm{T}},\end{aligned} \tag{1}$$

with angles $\nu(t)$ describing the elastic deformations of the tower, angle β representing bending of the jib in radial direction (rigid-body motion) and $v(x_{\mathrm{j}}, t)$ describes bending of the jib in slewing/tangential direction. $\varphi_x(t)$ and $\varphi_y(t)$ are the upper, and $\phi_x(t)$ and $\phi_y(t)$ are the lower pendulum angles whereas x_{j} is a spatial coordinate.

To derive the kinematic relations, four different Cartesian coordinate systems are introduced: the jib-fixed local frame (${}^{\mathrm{J}}\mathbf{x}$, coordinates: x_{j}, y_{j}, z_{j}), the tower-fixed local frame (${}^{\mathrm{T}}\mathbf{x}$, x_{t}, y_{t}, z_{t}), the platform-fixed rotating frame (${}^{\mathrm{R}}\mathbf{x}$, x_{r}, y_{r}, z_{r}), and the Newtonian (inertial) frame (${}^{\mathrm{N}}\mathbf{x}$ or just $\mathbf{x}$, coordinates: x_{n}, y_{n}, z_{n}) with arbitrary vector $\mathbf{x}$, see Fig. 1.

The transformations from the jib to the tower frame

$${}^{\mathrm{T}}\mathbf{x} = \underbrace{\mathbf{R}_{z,\nu_z}\left(\mathbf{R}_{x,\nu_x}\mathbf{R}_{y,(\alpha_{\mathrm{j}}-\alpha_{\mathrm{t}})}\right)}_{:=\mathbf{R}_{\mathrm{jt}}} {}^{\mathrm{J}}\mathbf{x} + \mathbf{R}_{y,\nu_y}\mathbf{R}_{x,\nu_x}\begin{bmatrix}0\\0\\h_{\mathrm{tu}}\end{bmatrix}\Bigg), \tag{2}$$

from the tower to the rotating frame

$${}^{\mathrm{R}}\mathbf{x} = \mathbf{R}_{y,\alpha_{\mathrm{t}}}\left({}^{\mathrm{T}}\mathbf{x} + [0,0,h_{\mathrm{tl}}]^{\mathrm{T}}\right), \tag{3}$$

and from the rotating frame to the Newtonian frame

$${}^{\mathrm{N}}\mathbf{x} = \mathbf{R}_{z,\gamma}\left({}^{\mathrm{R}}\mathbf{x} + [r,0,0]^{\mathrm{T}}\right) \tag{4}$$

are expressed using Cardan angles with the elementary rotation matrices

$$\mathbf{R}_{x,\theta} = \begin{bmatrix}1 & 0 & 0\\ 0 & \cos(\theta) & -\sin(\theta)\\ 0 & \sin(\theta) & \cos(\theta)\end{bmatrix}, \tag{5}$$

$$\mathbf{R}_{y,\theta} = \begin{bmatrix}\cos(\theta) & 0 & \sin(\theta)\\ 0 & 1 & 0\\ -\sin(\theta) & 0 & \cos(\theta)\end{bmatrix}, \tag{6}$$

and

$$\mathbf{R}_{z,\theta} = \begin{bmatrix}\cos(\theta) & -\sin(\theta) & 0\\ \sin(\theta) & \cos(\theta) & 0\\ 0 & 0 & 1\end{bmatrix}. \tag{7}$$

The center of mass of the tower's lower part

$${}^{\mathrm{R}}\mathbf{r}_{\mathrm{tl}} = \mathbf{R}_{y,\alpha_t}\,[0,0,s_{\mathrm{tl}}]^{\mathrm{T}} \tag{8}$$

in the rotating frame and of its upper part

$${}^{\mathrm{T}}\mathbf{r}_{\mathrm{tu}} = \mathbf{R}_{z,\nu_z}\,\mathbf{R}_{y,\nu_y}\,\mathbf{R}_{x,\nu_x}\,[0,0,s_{\mathrm{tu}}]^{\mathrm{T}} \tag{9}$$

in the tower frame are expressed using matrices (5), (6), and (7). Points at the jib in the local jib frame are

$${}^{\mathrm{J}}\mathbf{r}_{\mathrm{j}} = \mathbf{R}_{y,\beta}\,[x_{\mathrm{j}}, v\,(x_{\mathrm{j}}, t)\,, 0]^{\mathrm{T}}. \tag{10}$$

The trolley position $\mathbf{x}_{\mathrm{tr}}$ is determined by $x_{\mathrm{j}} = x_{\mathrm{tr}}$ and is used to calculate the hook position

$${}^{\mathrm{R}}\mathbf{r}_{\mathrm{h}} = {}^{\mathrm{R}}\mathbf{r}_{\mathrm{tr}} - \mathbf{R}_{\varphi_y}\,\mathbf{R}_{\varphi_x}\,[0,0,l]^{\mathrm{T}} \tag{11}$$

in the rotating frame. It yields the payload position

$${}^{\mathrm{R}}\mathbf{r}_{\mathrm{pl}} = {}^{\mathrm{R}}\mathbf{r}_{\mathrm{h}} - \mathbf{R}_{\phi_y}\,\mathbf{R}_{\phi_x}\,[0,0,l_{\mathrm{dp}}]^{\mathrm{T}} \tag{12}$$

and the counter weight's position is

$${}^{\mathrm{R}}\mathbf{r}_{\mathrm{cw}} = [-x_{\mathrm{cw}}, 0, z_{\mathrm{cw}}]^{\mathrm{T}}. \tag{13}$$

The lower part of the tower is fixed at the crane platform and its angular velocity is

$${}^{\mathrm{N}}\boldsymbol{\omega}_{\mathrm{tl}} = [0,0,\dot{\gamma}]^{\mathrm{T}} \tag{14}$$

whereas the tower's upper part additionally rotates due to elastic deformations which yields the angular velocity

$${}^{\mathrm{N}}\boldsymbol{\omega}_{\mathrm{tu}} = \begin{bmatrix}0\\0\\\dot{\gamma}\end{bmatrix} + \mathbf{R}_{z,\gamma}\mathbf{R}_{y,\alpha_{\mathrm{t}}}\left(\begin{bmatrix}0\\0\\\dot{\nu}_z\end{bmatrix} + \mathbf{R}_{z,\nu_z}\left(\begin{bmatrix}0\\\dot{\nu}_y\\0\end{bmatrix} + \mathbf{R}_{y,\nu_y}\begin{bmatrix}\dot{\nu}_x\\0\\0\end{bmatrix}\right)\right). \tag{15}$$

The angular velocity of the jib is

$$ {}^{\mathrm{N}}\boldsymbol{\omega}_{\mathrm{j}} = \begin{bmatrix} 0 \\ 0 \\ \dot{\gamma} \end{bmatrix} + \mathbf{R}_{z,\gamma}\mathbf{R}_{y,\alpha_t}\left(\begin{bmatrix} 0 \\ 0 \\ \dot{\nu}_z \end{bmatrix} + \mathbf{R}_{z,\nu_z}\mathbf{R}_{y,\nu_y} \begin{bmatrix} \dot{\nu}_x \\ 0 \\ 0 \end{bmatrix} + \mathbf{R}_{\mathrm{jt}} \begin{bmatrix} 0 \\ \dot{\beta} \\ 0 \end{bmatrix} \right). \tag{16} $$

2.2 Energy expressions

The mass inertia tensors of the jib

$$ {}^{\mathrm{J}}\boldsymbol{\Theta}_{\mathrm{j}} = \begin{bmatrix} \Theta_{1\mathrm{j}} & 0 & 0 \\ 0 & \Theta_{2\mathrm{j}} & 0 \\ 0 & 0 & \Theta_{3\mathrm{j}} \end{bmatrix} \tag{17} $$

and of the tower

$$ {}^{\mathrm{T}}\boldsymbol{\Theta}_{\mathrm{tu}} = \begin{bmatrix} \Theta_{1\mathrm{tu}} & 0 & 0 \\ 0 & \Theta_{2\mathrm{tu}} & 0 \\ 0 & 0 & \Theta_{3\mathrm{tu}} \end{bmatrix} \tag{18} $$

and

$$ {}^{\mathrm{T}}\boldsymbol{\Theta}_{\mathrm{tl}} = \begin{bmatrix} \Theta_{1\mathrm{tl}} & 0 & 0 \\ 0 & \Theta_{2\mathrm{tl}} & 0 \\ 0 & 0 & \Theta_{3\mathrm{tl}} \end{bmatrix} \tag{19} $$

are determined in local coordinate frames. Using the transformations (2), (3), and (4) yields the mass moments of inertia of the jib

$$ {}^{\mathrm{N}}\boldsymbol{\Theta}_{\mathrm{j}} = \mathbf{R}_{\Theta_{\mathrm{nj}}}\, {}^{\mathrm{J}}\boldsymbol{\Theta}_{\mathrm{j}}\, \mathbf{R}_{\Theta_{\mathrm{nj}}}^{\mathrm{T}} \tag{20} $$

with $\mathbf{R}_{\Theta_{\mathrm{nj}}} = \mathbf{R}_{z,\gamma}\mathbf{R}_{y,\alpha_t}\mathbf{R}_{\mathrm{jt}}\mathbf{R}_{y,\beta}$ of tower's upper part

$$ {}^{\mathrm{N}}\boldsymbol{\Theta}_{\mathrm{tu}} = \mathbf{R}_{\Theta_{\mathrm{ntu}}}\, {}^{\mathrm{T}}\boldsymbol{\Theta}_{\mathrm{tu}}\, \mathbf{R}_{\Theta_{\mathrm{ntu}}}^{\mathrm{T}} \tag{21} $$

with $\mathbf{R}_{\Theta_{\mathrm{ntu}}} = \mathbf{R}_{z,\gamma}\mathbf{R}_{y,\alpha_t}\mathbf{R}_{z,\nu_z}\,\mathbf{R}_{y,\nu_y}\,\mathbf{R}_{x,\nu_x}$ and of tower's lower part

$$ {}^{\mathrm{N}}\boldsymbol{\Theta}_{\mathrm{tl}} = \mathbf{R}_{z,\gamma}\,\mathbf{R}_{y,\alpha_t}\, {}^{\mathrm{T}}\boldsymbol{\Theta}_{\mathrm{tl}}\, \mathbf{R}_{y,\alpha_t}^{\mathrm{T}}\,\mathbf{R}_{z,\gamma}^{\mathrm{T}} \tag{22} $$

in the Newtonian frame. The total kinetic energy consists of the translational part

$$ \begin{aligned} T_{\mathrm{trans}} = \frac{1}{2}\Big(& m_{\mathrm{cw}}\,\dot{\mathbf{r}}_{\mathrm{cw}}^{\mathrm{T}}\,\dot{\mathbf{r}}_{\mathrm{cw}} + m_{\mathrm{tr}}\,\dot{\mathbf{r}}_{\mathrm{tr}}^{\mathrm{T}}\,\dot{\mathbf{r}}_{\mathrm{tr}} + m_{\mathrm{h}}\,\dot{\mathbf{r}}_{\mathrm{h}}^{\mathrm{T}}\,\dot{\mathbf{r}}_{\mathrm{h}} \\ & + m_{\mathrm{pl}}\,\dot{\mathbf{r}}_{\mathrm{pl}}^{\mathrm{T}}\,\dot{\mathbf{r}}_{\mathrm{pl}} + m_{\mathrm{tl}}\,\dot{\mathbf{r}}_{\mathrm{tl}}^{\mathrm{T}}\,\dot{\mathbf{r}}_{\mathrm{tl}} + m_{\mathrm{tu}}\,\dot{\mathbf{r}}_{\mathrm{tu}}^{\mathrm{T}}\,\dot{\mathbf{r}}_{\mathrm{tu}} \\ & + \int_0^{l_{\mathrm{j}}} \mu_{\mathrm{j}}\,\dot{\mathbf{r}}_{\mathrm{j}}^{\mathrm{T}}\,\dot{\mathbf{r}}_{\mathrm{j}}\,\mathrm{d}x_{\mathrm{j}} \Big) \end{aligned} \tag{23} $$

and the rotational part

$$ T_{\mathrm{rot}} = \frac{1}{2}\left(\boldsymbol{\omega}_{\mathrm{tl}}^{\mathrm{T}}\,\boldsymbol{\Theta}_{\mathrm{tl}}\,\boldsymbol{\omega}_{\mathrm{tl}} + \boldsymbol{\omega}_{\mathrm{tu}}^{\mathrm{T}}\,\boldsymbol{\Theta}_{\mathrm{tu}}\,\boldsymbol{\omega}_{\mathrm{tu}} + \boldsymbol{\omega}_{\mathrm{j}}^{\mathrm{T}}\,\boldsymbol{\Theta}_{\mathrm{j}}\,\boldsymbol{\omega}_{\mathrm{j}} \right), \tag{24} $$

whereas the total potential energy consists of parts due to gravitation

$$ \begin{aligned} U_{\mathrm{g}} = g\Big(& m_{\mathrm{cw}}\,\mathbf{r}_{\mathrm{cw}}^{\mathrm{T}} + m_{\mathrm{tr}}\,\mathbf{r}_{\mathrm{tr}}^{\mathrm{T}} + m_{\mathrm{h}}\,\mathbf{r}_{\mathrm{h}}^{\mathrm{T}} + m_{\mathrm{pl}}\,\mathbf{r}_{\mathrm{pl}}^{\mathrm{T}} \\ & + m_{\mathrm{tl}}\,\mathbf{r}_{\mathrm{tl}}^{\mathrm{T}} + m_{\mathrm{tu}}\,\mathbf{r}_{\mathrm{tu}}^{\mathrm{T}} + \int_0^{l_{\mathrm{j}}} \mu_{\mathrm{j}}\,\mathbf{r}_{\mathrm{j}}^{\mathrm{T}}\mathrm{d}x_{\mathrm{j}} \Big)\mathbf{e}_z \end{aligned} \tag{25} $$

and due to elastic deformations

$$ \begin{aligned} U_{\mathrm{el}} = & \frac{1}{2}\left(c_{\mathrm{t}z}\,\nu_z^2 + c_{\mathrm{t}y}\,\nu_y^2 + c_{\mathrm{t}x}\,\nu_x^2 + c_{\mathrm{j}y}\,\beta^2 \right) \\ & + \frac{1}{2}\int_0^{l_{\mathrm{j}}} E_{\mathrm{j}}\,I_{zz,\mathrm{j}} \left(\frac{\partial^2 v}{\partial x_{\mathrm{j}}^2} \right)^2 \mathrm{d}x_{\mathrm{j}}. \end{aligned} \tag{26} $$

2.3 Discretization with Ritz method

The jib's deformation in slewing direction $v(x,t)$, which is modeled by a cantilever beam, is discretized applying Ritz's method, see e.g. Hagedorn and DasGupta (2007). The ansatz

$$ v(x_{\mathrm{j}},t) = \Psi_1(x_{\mathrm{j}})\,q_{v1}(t) + \Psi_2(x_{\mathrm{j}})\,q_{v2}(t) \tag{27} $$

yields two degrees of freedom $q_{v1}(t)$ and $q_{v2}(t)$. Both shape functions Ψ_1 and Ψ_2 have to satisfy the geometric boundary conditions

$$ \Psi_i(0) = 0 \quad \text{and} \quad \left.\frac{\mathrm{d}\Psi_i}{\mathrm{d}x_{\mathrm{j}}}\right|_{x_{\mathrm{j}}=0} = 0, \quad i \in 1,2. \tag{28} $$

Additionally, they are assumed to satisfy the dynamic boundary conditions

$$ \left.\frac{\mathrm{d}^2\Psi_i}{\mathrm{d}x_{\mathrm{j}}^2}\right|_{x_{\mathrm{j}}=l_{\mathrm{j}}} = 0 \quad \text{and} \quad \left.\frac{\mathrm{d}^3\Psi_i}{\mathrm{d}x_{\mathrm{j}}^3}\right|_{x_{\mathrm{j}}=l_{\mathrm{j}}} = 0, \quad i \in 1,2 \tag{29} $$

and condition

$$ \Psi_i(l_{\mathrm{j}}) = \Psi_{li}, \quad i \in 1,2, \tag{30} $$

which is used to normalize shape functions Ψ_1 and Ψ_2. This is necessary to compare them with eigenvectors e.g. resulting from a finite element analysis (FEA). Besides (28), (29), and (30), the conditions

$$ \left.\frac{\mathrm{d}^3\Psi_1}{\mathrm{d}x_j^3}\right|_{x_{\mathrm{j}}=\bar{x}_1 l_j} = 0,\ \Psi_2(\bar{x}_2 l_j) = 0 \text{ and } \left.\frac{\mathrm{d}^2\Psi_2}{\mathrm{d}x_{\mathrm{j}}^2}\right|_{x_{\mathrm{j}}=\bar{x}_3 l_j} = 0 \tag{31} $$

are used to introduce additional parameters $\bar{x}_1$, $\bar{x}_2$ and $\bar{x}_3$. Both shape functions

$$ \begin{aligned} \Psi_1(x_{\mathrm{j}}) = & a_{11}\left(\frac{x_{\mathrm{j}}}{l_{\mathrm{j}}}\right)^5 + a_{12}\left(\frac{x_{\mathrm{j}}}{l_{\mathrm{j}}}\right)^4 \\ & + a_{13}\left(\frac{x_{\mathrm{j}}}{l_{\mathrm{j}}}\right)^3 + a_{14}\left(\frac{x_{\mathrm{j}}}{l_{\mathrm{j}}}\right)^2 \end{aligned} \tag{32} $$

and

$$ \begin{aligned} \Psi_2(x_{\mathrm{j}}) = & a_{21}\left(\frac{x_{\mathrm{j}}}{l_{\mathrm{j}}}\right)^6 + a_{22}\left(\frac{x_{\mathrm{j}}}{l_{\mathrm{j}}}\right)^5 + a_{23}\left(\frac{x_{\mathrm{j}}}{l_{\mathrm{j}}}\right)^4 \\ & + a_{24}\left(\frac{x_{\mathrm{j}}}{l_{\mathrm{j}}}\right)^3 + a_{25}\left(\frac{x_{\mathrm{j}}}{l_{\mathrm{j}}}\right)^2 \end{aligned} \tag{33} $$

are chosen to be polynomial. The conditions (28)-(31) lead to two matrix equations

$$ \begin{bmatrix} 20 & 12 & 6 & 2 \\ 60 & 24 & 6 & 0 \\ 60\,\bar{x}_1^2 & 24\,\bar{x}_1 & 6 & 0 \\ 1 & 1 & 1 & 1 \end{bmatrix} \begin{bmatrix} a_{11} \\ a_{12} \\ a_{13} \\ a_{14} \end{bmatrix} = \begin{bmatrix} 0 \\ 0 \\ 0 \\ \Psi_{l1} \end{bmatrix}, \tag{34} $$

and

$$ \begin{bmatrix} 30\,\bar{x}_3^4 & 20\,\bar{x}_3^3 & 12\,\bar{x}_3^2 & 6\,\bar{x}_3 & 2 \\ \bar{x}_2^6 & \bar{x}_2^5 & \bar{x}_2^4 & \bar{x}_2^3 & \bar{x}_2^2 \\ 30 & 20 & 12 & 6 & 2 \\ 120 & 60 & 24 & 6 & 0 \\ 1 & 1 & 1 & 1 & 1 \end{bmatrix} \begin{bmatrix} a_{21} \\ a_{22} \\ a_{23} \\ a_{24} \\ a_{25} \end{bmatrix} = \begin{bmatrix} 0 \\ 0 \\ 0 \\ 0 \\ \Psi_{l2} \end{bmatrix} \tag{35} $$

to calculate the coefficients in (32) and (33). The resulting symbolical terms are quite lengthy and therefore omitted here. The parameters $\bar{x}_1$, $\bar{x}_2$ and $\bar{x}_3$ in those terms are used to fit the polynomials to shape functions resulting from a FEA by optimization.

2.4 Equations of motion

The Lagrangian formalism is applied to derive the equations of motion. Lagrange's equations of second kind read

$$ \frac{\mathrm{d}}{\mathrm{d}t}\frac{\partial \mathscr{L}}{\partial\, \dot{\mathbf{q}}_{\mathrm{m}}} - \frac{\partial \mathscr{L}}{\partial\, \mathbf{q}_{\mathrm{m}}} = 0 \tag{36} $$

with the Lagrangian $\mathscr{L} = T_{\mathrm{trans}} + T_{\mathrm{rot}} - U_{\mathrm{g}} - U_{\mathrm{el}}$, which is the difference between total kinetic and potential energy. Besides (1), the rotational angle of the crane

platform $\gamma(t)$, the trolley position $x_{\mathrm{tr}}(t)$ and the rope length $l(t)$ are introduced, which are all driven by electrical drives. The resulting equations of motion are quite lengthy and therefore omitted in this paper. The matrix structure of these equations is

$$\mathbf{M}(\mathbf{q}_{\mathrm{m}})\,\ddot{\mathbf{q}}_{\mathrm{m}} + \mathbf{k}\,(\mathbf{q}_{\mathrm{m}}, \mathbf{q}_{\mathrm{a}}, \dot{\mathbf{q}}_{\mathrm{m}}, \dot{\mathbf{q}}_{\mathrm{a}}) = \mathbf{B}_u \ddot{\mathbf{q}}_{\mathrm{a}} \tag{37}$$

with $\mathbf{q}_{\mathrm{a}} = [\gamma \;\; x_{\mathrm{tr}} \;\; l]^{\mathrm{T}}$. For simulations, the explicit form of these equations is determined by inverting the mass matrix $\mathbf{M}$ numerically. To analyze the dynamical behavior of the crane structure, (37) is linearized around the position of rest $\mathbf{q}_0$ calculated by

$$\mathbf{k}\,(\mathbf{q}_{\mathrm{m}}, \mathbf{q}_{\mathrm{a}}, \mathbf{0}, \mathbf{0}) = \mathbf{0}. \tag{38}$$

In $\mathbf{q}_0$ only the mechanical degrees of freedom ν_y and β in radial direction are unequal to zero because all forces act in tower-jib-plane. The linear equations of motion

$$\underbrace{\mathbf{M}(\mathbf{q}_0)}_{\mathbf{M}_{\mathrm{lin}}}\,\ddot{\mathbf{q}}_{\mathrm{lin}} + \underbrace{\left.\frac{\partial \mathbf{k}}{\partial \mathbf{q}}\right|_{\dot{\mathbf{q}}=\mathbf{0},\mathbf{q}_0}}_{\mathbf{K}_{\mathrm{lin}}}\,\mathbf{q}_{\mathrm{lin}} = \underbrace{\mathbf{B}_u(\mathbf{q}_0)}_{\mathbf{B}_{\mathrm{lin}}}\,\ddot{\mathbf{q}}_{\mathrm{a}} \tag{39}$$

with $\mathbf{q}^{\mathrm{T}} = \left[\mathbf{q}_{\mathrm{m}} \;\; \mathbf{q}_{\mathrm{a}}^{\mathrm{T}}\right]^{\mathrm{T}}$ and $\mathbf{q}_{\mathrm{lin}} = \mathbf{q} - \mathbf{q}_0$ are derived symbolically. These equations are used for the modal analysis in Section 4 and can be used for linear control design. Notice, that $v(x_{\mathrm{j}}, t)$ is replaced by q_{v1} and q_{v2}. Since all coupling forces (Coriolis and centrifugal) are nonlinear, the linear equations of motion are decoupled and the motions are distinguished in radial (tower-jib-plane) and slewing direction. A transformation yields the first order differential equation

$$\begin{bmatrix}\dot{\mathbf{q}}\\ \ddot{\mathbf{q}}\end{bmatrix} = \begin{bmatrix}\mathbf{0} & \mathbf{I}\\ \mathbf{M}_{\mathrm{lin}}^{-1}\mathbf{K}_{\mathrm{lin}} & \mathbf{M}_{\mathrm{lin}}^{-1}\mathbf{D}_{\mathrm{mod}}\end{bmatrix}\begin{bmatrix}\mathbf{q}\\ \dot{\mathbf{q}}\end{bmatrix} + \begin{bmatrix}\mathbf{0}\\ \mathbf{B}_{\mathrm{lin}}\end{bmatrix}\ddot{\mathbf{q}}_{\mathrm{a}}. \tag{40}$$

Varying the modal damping ratios of the modes describing the structural deflections, see Fig. 2 (b),(d),(f), and (g), up to 0.1 in simulation, showed that small damping does not have a significant influence on the natural frequencies. Therefore $\mathbf{D}_{\mathrm{mod}} = \mathbf{0}$ is assumed for the modal analysis.

3. PARAMETRIZATION AND OPTIMIZATION

Tower and jib have piecewise constant parameters because they consist of different segments which itself have constant parameters. Crane manufacturers usually perform a finite element analysis (FEA) with thousands of degrees of freedom to verify structural durability. Therefore, it is assumed that results from FEA are available to determine the missing parameters. If this is not the case, a FEA of tower and jib can be performed using Euler-Bernoulli-beam elements and linear elements with two nodes and linear shape functions can be used for (tower) torsion. Moreover, the material and geometry data of the different segments of tower and jib are available. In the following, the area moments of inertia I, Young's moduli E, densities ρ, masses m, centers of mass, lengths l, and cross-sectional areas A of the different segments are assumed to be known. However, these parameters cannot be used directly in the derived model. Whereas the inertia parameters result from the geometry and densities, the stiffnesses c and area moment of inertia $I_{zz,\mathrm{j}}$ are more challenging. Therefore, those parameters are determined by numerical optimization using measurement data. In the following, all model parameters are expressed by known parameters.

The joint's position between the two tower segments is chosen to be $h_{\mathrm{tl}} = 0.272\,l_{\mathrm{t}}$, suggested by Dresig and Fidlin (2014) for homogeneous Euler-Bernoulli-beams, although tower's parameters are only piecewise constant. The principal mass moments of inertia of the tower

$$\Theta_{1\mathrm{t}} = \sum_i^{N_{\mathrm{t}}} \rho_{\mathrm{t},i}\,l_{\mathrm{t},i}\left(I_{xx,\mathrm{t},i} + \frac{A_{\mathrm{t},i}}{3}l_{\mathrm{t},i}^2\right), \tag{41}$$

$$\Theta_{2\mathrm{t}} = \sum_i^{N_{\mathrm{t}}} \rho_{\mathrm{t},i}\,l_{\mathrm{t},i}\left(I_{yy,\mathrm{t},i} + \frac{A_{\mathrm{t},i}}{3}l_{\mathrm{t},i}^2\right), \tag{42}$$

$$\Theta_{3\mathrm{t}} = \sum_i^{N_{\mathrm{t}}} \rho_{\mathrm{t},i}\,l_{\mathrm{t},i}\,\left(I_{xx,\mathrm{t},i} + I_{yy,\mathrm{t},i}\right), \tag{43}$$

and of the jib

$$\Theta_{1\mathrm{j}} = \sum_i^{N_j} \rho_{\mathrm{j},i}\,l_{\mathrm{j},i}\,\left(I_{yy,\mathrm{j},i} + I_{zz,\mathrm{j},i}\right), \tag{44}$$

$$\Theta_{2\mathrm{j}} = \sum_i^{N_{\mathrm{j}}} \rho_{\mathrm{j},i}\,l_{\mathrm{j},i}\left(I_{yy,\mathrm{j},i} + \frac{A_{\mathrm{j},i}}{3}l_{\mathrm{j},i}^2\right), \tag{45}$$

$$\Theta_{3\mathrm{j}} = \sum_i^{N_{\mathrm{j}}} \rho_{\mathrm{j},i}\,l_{\mathrm{j},i}\left(I_{zz,\mathrm{j},i} + \frac{A_{\mathrm{j},i}}{3}l_{\mathrm{j},i}^2\right) \tag{46}$$

depend on the known parameters of the N_{t} tower and N_{j} jib segments. The mass moments of inertia of jib and tower's upper part are calculated in the jib and the tower coordinate frames with respect to their origin, see Fig. 1. For tower's lower part the principal mass moments of inertia are calculated with respect to the origin of the rotating frame. The mass per length of the jib

$$\mu_{\mathrm{j}}(x_{\mathrm{j}}) = \left(\frac{12\,m_{\mathrm{j}}\,s_{\mathrm{j}}}{l_{\mathrm{j}}^3} - \frac{6\,m_{\mathrm{j}}}{l_{\mathrm{j}}^2}\right)x_{\mathrm{j}} + \left(\frac{4\,m_{\mathrm{j}}}{l_{\mathrm{j}}} - \frac{6\,m_{\mathrm{j}}\,s_{\mathrm{j}}}{l_{\mathrm{j}}^2}\right), \tag{47}$$

is chosen such, that the total mass m_{j} and the center of mass s_{j} of the jib are described accordingly.

For optimization of the stiffness parameter initial values are needed. Since the natural frequencies ω of the isolated bodies (tower and jib) are available from FEA, they are used to estimate these parameter. The stiffnesses of the tower are

$$c_{\mathrm{t}x} = \omega_{\mathrm{t}x}^2\,\left(\Theta_{1\mathrm{tu}} + m_{\mathrm{tu}}\,s_{\mathrm{tu}}^2\right), \tag{48}$$

$$c_{\mathrm{t}y} = \omega_{\mathrm{t}y}^2\,\left(\Theta_{2\mathrm{tu}} + m_{\mathrm{tu}}\,s_{\mathrm{tu}}^2\right), \tag{49}$$

and

$$c_{\mathrm{t}z} = \omega_{\mathrm{t}z}^2\,\Theta_{3\mathrm{tu}}. \tag{50}$$

Jib's stiffness in radial direction

$$c_{\mathrm{j}y} = \left(\frac{1}{\omega_{\mathrm{j}y}^2\left(\Theta_{2\mathrm{j}} + m_{\mathrm{j}}\,s_{\mathrm{j}}^2\right)} + \frac{1}{c_{\mathrm{g}}}\right)^{-1} \tag{51}$$

depends on the natural frequency for jib bending $\omega_{\mathrm{j}y}$ and the stiffness of the guying c_g, which typically consists of rods and ropes. The first is assumed to be available from FEA and the latter is calculated with the unit deformation method assuming a rigid crane structure and elastic springs for the guying. Alternatively, the stiffness of the most elastic rope or rod of the guying is a good guess.

The optimization variables in (32) and (33) are calculated next. We decided to determine the zero $\bar{x}_2$ graphically plotting the second eigenvector, which is calculated by a FEA using Euler-Bernoulli-beam elements. The parameters $\bar{x}_1$

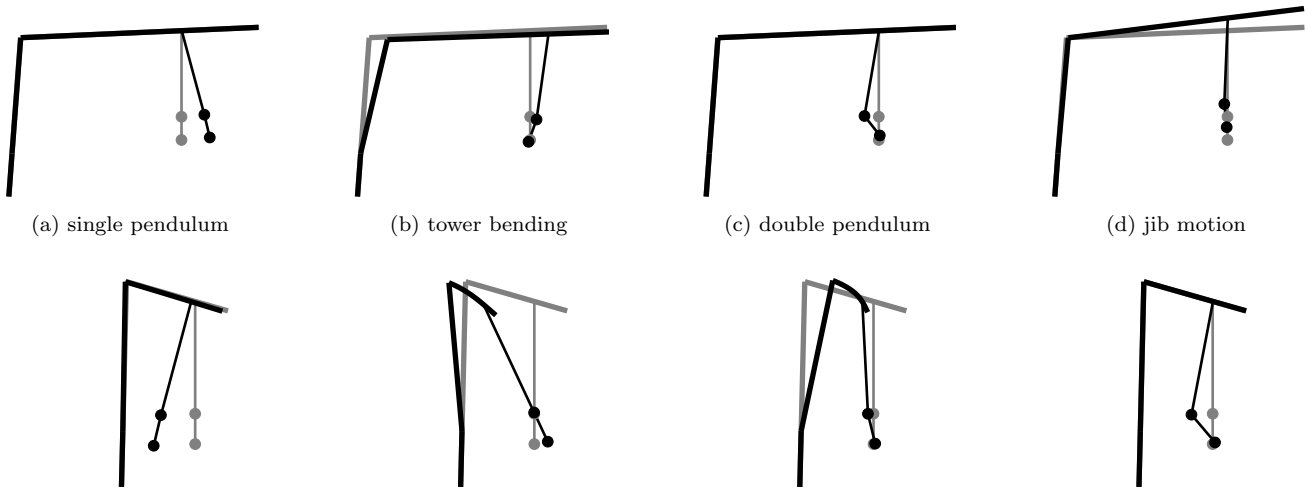

(a) single pendulum (b) tower bending (c) double pendulum (d) jib motion

(e) single pendulum (f) tower torsion (g) tower bending (h) double pendulum

Fig. 2. Mode shapes of a self-erecting tower crane in radial (a-d) and slewing direction (e-h).

and $\bar{x}_3$ are determined by optimization using a nonlinear least square algorithm minimizing

$$F = \sum_{k}^{N_{\text{fem}}} \left(\Psi_i\left(x_k\right) - \tilde{v}\left(x_k\right)\right)^2, \quad i \in 1,2 \tag{52}$$

where $\tilde{v}$ is the deformation of the node at position x_k from a finite element analysis of the jib using in total N_{fem} nodes. The jib's area moment of inertia

$$I_{zz,\text{j}} = \frac{\mathbf{q}_1^{\text{T}}\mathbf{K}_{\text{j,fem}}\,\mathbf{q}_1 + \mathbf{q}_2^{\text{T}}\mathbf{K}_{\text{j,fem}}\,\mathbf{q}_2}{\int_0^{l_\text{j}} E_\text{j}\left(\Psi_1''\right)^2\,\text{d}x_\text{j} + \int_0^{l_\text{j}} E_\text{j}\left(\Psi_2''\right)^2\,\text{d}x_\text{j}} \tag{53}$$

is calculated by the equivalence of elastic deformation energy due to bending of the jib. Therefore, the stiffness matrix $\mathbf{K}_{\text{j,fem}}$ and the first two eigenvectors $\mathbf{q}_1$ and $\mathbf{q}_2$ are calculated applying the finite element method. Finally, experimental data is used for optimization of the stiffness parameters c and $I_{zz,\text{j}}$ by solving

$$\min \sum_{k=1}^{N} \det\left(\mathbf{K}_{\text{lin}} - \omega_{k,\text{meas}}^2\,\mathbf{M}_{\text{lin}}\right)^2 \tag{54}$$

with measured frequencies $\omega_{k,\text{meas}}$ using a nonlinear least squares algorithm again. Thereby, only the natural frequencies of the structure are considered and those of the pendulum motions are neglected in the objective function (54). The optimization parameters are constrained to avoid resulting stiffnesses which are unrealistic. Additionally, the payload mass m_{pl} and the rope length l are chosen large enough to avoid that the order of the frequencies change for different stiffness values during numerical optimization.

4. MODAL ANALYSIS AND VALIDATION

In the following, a modal analysis is applied and the results are compared with measurement data. To determine the natural frequencies experimentally, an industrial tower crane was equipped with inertia measurement units located at jib's and tower's tip. The crane structure was excited in radial direction either by lifting a payload from the ground or by setting it down. Thereby, the payload's gravitation force acting on the crane structure changes very fast, which leads to large structural vibrations. To achieve an excitation in slewing direction, the tower crane was rapidly stopped from a constant rotation speed using the emergency stop. In both cases, the natural frequencies are determined applying a Fast Fourier Transform to the measured angular velocities and accelerations.

To calculate the natural frequencies and mode shapes using the dynamical model, the ansatz $\mathbf{q}_{\text{lin}} = \hat{\mathbf{q}}_{\text{lin}}\,e^{i\omega t}$ is substituted into (39). Assuming $\ddot{\mathbf{q}}_{\text{a}} = \mathbf{0}$ yields the eigenvalue problem

$$\left(\mathbf{K}_{\text{lin}} - \omega_k^2\,\mathbf{M}_{\text{lin}}\right)\hat{\mathbf{q}}_k = \mathbf{0} \tag{55}$$

for k natural frequencies ω_k and eigenvectors $\hat{\mathbf{q}}_k$. Solving this problem numerically leads to the mode shapes shown in Fig. 2. The two mode shapes corresponding to the highest natural frequencies are not shown. They mainly describe bending of the jib in slewing direction and have significant higher corresponding natural frequencies than the other modes. However, those mode shapes are essential to describe the trolley position on the jib accordingly. Ignoring these mode shapes additionally yields too high natural frequencies which cannot be compensated modifying the stiffnesses.

In Fig. 3 and Fig. 4, the normalized frequencies $2\pi f\sqrt{\frac{l+l_{\text{dp}}}{g}}$ with $\omega = 2\pi f$ are plotted over the payload mass m_{pl} and the trolley position x_{tr} respectively. The natural frequencies strongly depend on the rope length l, payload mass m_{pl}, and trolley position x_{tr}. The single pendulum frequencies in radial and slewing direction mainly depends on the rope length (for cranes with rigid structure, the relation $\omega = \sqrt{\frac{g}{l}}$ holds). For elastic cranes, however, these frequencies decrease with increasing payload masses m_{pl} and trolley positions x_{tr} as simulations and measurements show. Besides, the pendulum frequency in slewing direction is lower than those in radial direction due to greater elastic deformations of the crane structure in this direction, see Fig. 3 and Fig. 4. The double pendulum frequencies, see Fig. 2(c) and (h) depend significantly on the ratio between hook mass m_{h} and payload mass m_{pl} as well as on the rope lengths l and l_{dp}. For heavy payloads, the double pendulum frequency grows with increasing payload mass m_{pl}, whereas for small m_{pl} similar to m_{h} the double pendulum frequency decreases with increasing payload mass, see Fig. 3. Compared to the pendulum

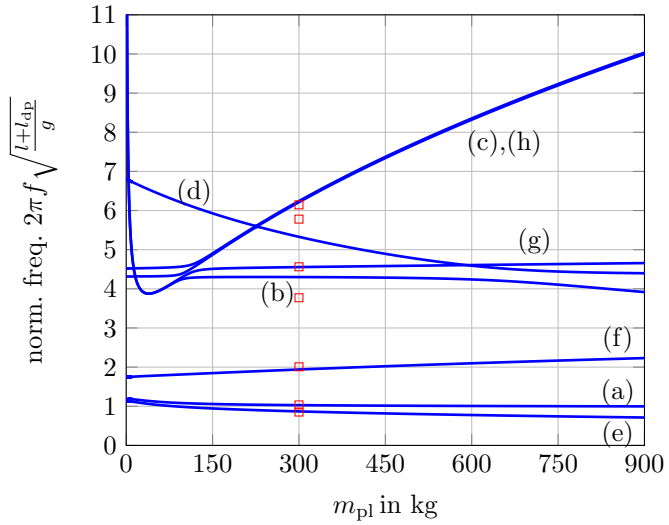

Fig. 3. Natural frequencies corresponding to the mode shapes shown in Fig. 2 from simulation (blue lines) and measurements (red squares) for trolley at the jib tip.

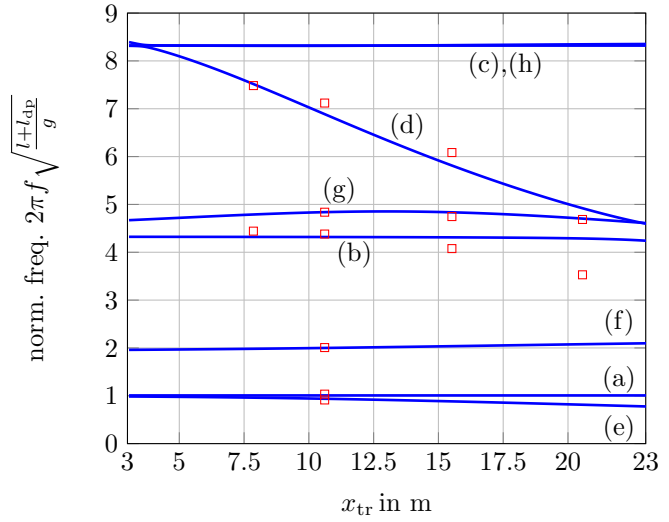

Fig. 4. Natural frequencies corresponding to the mode shapes shown in Fig. 2 from simulation (blue lines) and measurements (red squares) for a payload mass of 600 kg.

frequencies, most structural frequencies keep almost constant. The frequency corresponding to the mode shape shown in Fig. 2(d) significantly decreases with increasing payload mass and trolley positions. In the model, this effect is overstated, see Fig. 4(d). This is assumed not to be critical for control because this mode is hard to excite by the drives. Additionally, the frequency corresponding to the mode shape shown in Fig. 2(b) decreases for large trolley positions, which is not described by the model, see Fig. 4. Again, this is assumed not to be critical for control.

5. CONCLUSION

An elastic multi-body model of a bottom-slewing tower crane is derived considering the geometry of an self-erecting tower crane. The mode shapes and natural frequencies are analyzed via simulation and the results are compared with experimental data of an industrial tower crane. It is shown that the frequencies strongly depend on the rope length, trolley position, and payload mass. Especially, the pendulum frequencies in slewing and radial direction are different. This behavior cannot be described by a rigid crane model whereas the derived model describes these effects correctly. Although it is not assumed to be critical for anti-sway control, it might be desirable to model a crane specific guying in more detail to describe the frequencies in radial direction more accurate. This dynamical analysis of an industrial tower crane is part of an ongoing research project. In the next step, a feedback controller will be designed based on the derived multi-body model.

REFERENCES

Abdel-Rahman, E.M., Nayfeh, A.H., and Masoud, Z.N. (2003). Dynamics and control of cranes: A review. *J. Vib. Control*, 9(7), 863–908.

Arnold, E., Sawodny, O., Neupert, J., and Schneider, K. (2005). Anti-sway system for boom cranes based on a model predictive control approach. In *IEEE Int. Conf. on Mechatronics and Automation*, 1533–1538.

Devesse, W. (2012). *Slew control Methods for Tower Cranes*. Master's thesis, KTH Stockholm.

Dresig, H. and Fidlin, A. (2014). *Schwingungen mechanischer Antriebssysteme*. Springer, Berlin, Heidelberg.

Graichen, K., Egretzberger, M., and Kugi, A. (2010). Suboptimal model predictive control of a laboratory crane. *IFAC P. Ser.*, 43(14), 397–402.

Hagedorn, P. and DasGupta, A. (2007). *Vibrations and waves in continuous mechanical systems*. Wiley, Chichester.

Jerman, B., Podržaj, P., and Kramar, J. (2004). An investigation of slewing-crane dynamics during slewing motion – development and verification of a mathematical model. *Int. J. Mech. Sci.*, 46(5), 729–750.

Ju, F., Choo, Y.S., and Cui, F.S. (2006). Dynamic response of tower crane induced by the pendulum motion of the payload. *Int. J. Solids Struct.*, 43(2), 376–389.

Neupert, J., Hildebrandt, A., Sawodny, O., and Schneider, K. (2006). Trajectory tracking for boom cranes using a flatness based approach. In *SICE-ICASE Int. Joint Conf.*, 1812–1816.

Neupert, J., Arnold, E., Schneider, K., and Sawodny, O. (2010). Tracking and anti-sway control for boom cranes. *Control Eng. Pract.*, 18(1), 31–44.

Omar, H.M. and Nayfeh, A.H. (2003). Gain scheduling feedback control for tower cranes. *J. Vib. Control*, 9(3-4), 399–418.

Ramli, L., Mohamed, Z., Abdullahi, A.M., Jaafar, H.I., and Lazim, I.M. (2017). Control strategies for crane systems: A comprehensive review. *Mech. Syst. Signal Pr.*, 95, 1–23.

Rauscher, F. and Sawodny, O. (2017). An elastic jib model for the slewing control of tower cranes. *IFAC PapersOnLine*, 50(1), 9796–9801.

Rauscher, F. and Sawodny, O. (2020). Modeling and control of tower cranes with elastic structure. *IEEE T. Contr. Syst. T.*

Schlott, P., Rauscher, F., and Sawodny, O. (2016). Modelling the structural dynamics of a tower crane. In *IEEE Int. Conf. on Advanced Intelligent Mechatronics*, 763–768.

Takagi, K. and Nisimura, H. (1999). Gain-scheduled control of a tower crane considering varying load-rope length. *JSME Int. J. C-Mech. Sy.*, 42(4), 914–921.

Tinkir, M., Onen, U., Kalyoncu, M., and Sahin, Y. (2011). Modeling and control of scaled a tower crane system. In *3rd Int. Conf. on Computer Research and Development*, 93–98.

Vaughan, J., Kim, D., and Singhose, W. (2010). Control of tower cranes with double-pendulum payload dynamics. *IEEE T. Contr. Syst. T.*, 18(6), 1345–1358.

Yang, W., Zhang, Z., and Shen, R. (2007). Modeling of system dynamics of a slewing flexible beam with moving payload pendulum. *Mech. Res. Commun.*, 34(3), 260–266.

Zrnić, N. and Bošnjak, S. (2008). Comments on "modeling of system dynamics of a slewing flexible beam with moving payload pendulum". *Mech. Res. Commun.*, 35(8), 622–624.